batteries

MDPI

Article

Experimental Investigation on Thermal Runaway of Lithium-Ion Batteries under Low Pressure and Low Temperature

Di Meng, Jingwen Weng * and Jian Wang *

State Key Laboratory of Fire Science, University of Science and Technology of China, Hefei 230026, China; mengl@mail.ustc.edu.cn

* Correspondence: wengjw@mail.ustc.edu.cn (J.W.); wangj@ustc.edu.cn (J.W.)

Abstract: Understanding the thermal runaway mechanism of lithium-ion batteries under low pressure and low temperature is paramount for their application and transportation in the aviation industry. This work investigated the coupling effects of ambient pressure (100 kPa, 70 kPa, 40 kPa) and ambient temperature (−15 °C, 0 °C, 25 °C) on thermal behaviors in an altitude temperature chamber. The experimental results indicate that lowering ambient pressure and temperature could attenuate the thermal runaway intensity, which is mainly attributable to the reduction in oxygen concentration and the increase in heat loss. Such a dual effect leads to the maximum temperature decreasing from 811.9 °C to 667.5 °C, and the maximum temperature rate declines up to 2.6 times. Correspondingly, the whole thermal runaway process is deferred, the total time increases from 370 s to 503 s, and the time interval, Δt, from safety venting gains by 32.3% as the ambient pressure and temperature decrease. This work delivers an in-depth understanding of the thermal characteristics under low pressure and low temperature and provides meritorious guidance for the safety of cell transportation in aviation.

Keywords: lithium-ion battery; low pressure; low temperature; thermal runaway; thermal hazards

Citation: Meng, D.; Weng, J.; Wang, J. Experimental Investigation on Thermal Runaway of Lithium-Ion Batteries under Low Pressure and Low Temperature. *Batteries* **2024**, *10*, 243. https://doi.org/10.3390/batteries10070243

Academic Editors: Wojciech Mrozik and Vilas Pol

Received: 28 April 2024
Revised: 24 June 2024
Accepted: 4 July 2024
Published: 6 July 2024

1. Introduction

Global warming has become a serious environmental issue in recent years. Carbon reduction and carbon neutrality by 2050 have attracted considerable attention over the years. Countries around the world are vigorously developing renewable and sustainable energy sources, which are beneficial for decreasing carbon emissions. Lithium-ion batteries have recently been regarded as promising energy media and have been extensively applied in electric vehicles (EVs) at high plateau airports, in electric aircraft [1], and even in aerospace due to their outstanding merits of high energy density, extended cycle performance, and environmental friendliness [2,3]. For example, the Boeing 787 and Airbus 350 were the first commercial aircraft to utilize lithium-ion batteries as a power source. In addition, Beta's electric vertical take-off and landing (eVTOL) could complete a 621 km flight [4]. The application scenarios are becoming more extensive and sophisticated. Lithium-ion batteries are easily subjected to thermal runaway during air transportation when fresh cells are exposed to adverse conditions [5], which release substantial heat, accompanied by white smoke, jet fires, or even explosions [6]. Extensive previous work has been conducted and reported on the understanding of the electrochemical performance and structural degradation of electrode materials (both anodes and cathodes) [7] and electrolytes [8]. However, in recent years, lithium-ion battery accidents in aviation conditions have gradually increased, which may inhibit developments in the aviation industry [9]. According to statistics from the Federal Aviation Administration (FAA), more than 497 battery fires were reported in air transportation between 2006 and 2023 [10]. These catastrophic accidents have caused profound property loss and overshadowed the development of the aviation industry [11]. Therefore, it is imperative for us to intensively probe the thermal safety and characteristics of the thermal runaway of the lithium-ion battery under such conditions.

Generally, as the altitude increases, the ambient pressure and temperature decline gradually [12]. During air transportation, the cruising altitude for commercial airlines is in the range of 8000–10,000 m, where the external minimum pressure is approximately 26 kPa and the ambient temperature even reaches approximately −40 °C [13,14]. Therefore, the high-altitude environment, which is characterized by low pressure and low temperature, has an impact on thermal runaway characteristics. When lithium-ion batteries are subjected to accidents at high altitudes, they will be exposed to such conditions expediently. It has been reported that thermal runaway characteristics are influenced by many factors. For example, the cell SOC [15], cathode material [16], space distribution [3], and heating position [17]. However, the ambient pressure, which is directly associated with the oxygen concentration, also shows a pronounced effect on the thermal runaway process. Chen et al. [18] utilized in-situ calorimeters in Hefei (pressure, 100.8 kPa) and Lhasa (pressure, 64.3 kPa) to assess the thermal and fire hazards of lithium-ion batteries. Their results confirmed that reducing the ambient pressure caused a reduction in oxygen density, which resulted in an evident decrease in ignition time, mass loss, and combustion efficiency. Furthermore, Fu et al. [19] explained the lithium-ion battery venting process in detail through Darcy's law and Fick's law. Their results revealed that the ignition time and combustion intensity were weakened at low pressure, and the oxygen concentration gradient played an essential role in the internal active material decomposition and burning process during thermal runaway. In general, decreasing pressure means a decline in air density, which would further attenuate the natural convection heat loss. However, the research of Liu et al. [20] confirmed that the convective cooling effect is prominent during thermal runaway, and the relationship between the convection coefficient and ambient pressure can be expressed as $h \propto P^{0.2}$. In addition, the intensity of the internal side reaction is closely associated with the cathode material. Jia et al. [21] compared two typical cathode materials for lithium-ion batteries at various pressures. Their results indicated that even though the thermal runaway intensity weakened under low pressure, the thermal runaway time increased in $LiFePO_4$ batteries, whereas the thermal runaway decreased in $LiNi_{0.5}Co_{0.2}Mn_{0.3}$, illustrating the high complexity in distinctive low-pressure environments.

Many remarkable works have confirmed that ambient pressure shows significant effects on thermal runaway characteristics. However, lithium-ion batteries may confront more sophisticated environments under aviation conditions. Fundamentally, decreasing the ambient temperature relieves the internal chemical reaction of lithium-ion batteries. Niu et al. [22] found that the acceleration of the thermal runaway process between adjacent batteries was primarily attributed to the net convection transfer. Guo et al. [23] confirmed that the heating rates decreased as the ambient temperature declined, and a better heat dissipation condition at low temperatures could effectively migrate the temperature rate. In addition, Liu et al. [20] further explored the effects of ambient pressure and temperature on the thermal characteristics of a dimension linear arrangement lithium-battery module. The results indicated that the ambient pressure and temperature had little influence on the safety venting temperature and that the time interval between adjacent cells increased obviously. However, the effect of ambient temperature (between 23 °C and 33 °C) on the thermal runaway onset and maximum temperature was not clearly explained. During air transportation, lithium-ion batteries are more inclined to confront low-pressure and low-temperature conditions, which may further trigger domino accidents. Therefore, a systematical investigation related to the thermal runaway characteristics of lithium-ion batteries is urgently needed to meet the ever-increasing demand for aviation transportation and application.

This work endeavors to investigate the coupling effect of low pressure and low temperature on lithium-ion battery thermal characteristics. A set of experiments was arranged and conducted using 18,650 cylindrical lithium-ion batteries in a designed altitude temperature chamber. Three typical atmospheric pressures (101 kPa, 70 kPa, and 40 kPa) and ambient temperatures (−15 °C, 0 °C, and 25 °C) were selected. The thermal runaway characteristic parameters, including thermal runaway process images, critical temperature and time, and

mass loss, were measured and analyzed thoroughly. A scanning electron microscope (SEM) and energy-dispersive spectrometry (EDS) were utilized to identify the transformation electrode micromorphology and element composition of the cell electrode in different configurations. These experimental results are anticipated to deliver valuable references for the safety application and transportation of lithium-ion batteries in the aviation industry.

2. Experimental Platform and Setup

2.1. Battery Samples

The lithium-ion battery applied in this paper was a commercial 18,650 lithium-ion battery (height, 65 mm; diameter, 18 mm). Table 1 lists the battery specifications. The nominal capacity and voltage were 2600 mAh and 3.63 V, respectively. The cathode was nickel manganese cobalt oxide $LiNi_{0.5}Co_{0.2}Mn_{0.3}$ (NCM 523), and intercalation graphite was used as the anode. The cell mass was 44.8 ± 0.2 g after the plastic packing was peeled off. According to the product specifications, the storage temperature ranges from −20 to 60 °C for one month. Prior to the experiments, the cell was first discharged to 2.75 V with a constant current of 0.5 C. Then, the fresh cells were charged using the same constant current/constant voltage (CC-CV) method to 100% SOC three times. Finally, to minimize internal heat generation during the charging/discharging process and maintain a stable state, the cycled cells rested for at least 24 h.

Table 1. Technical specifications of the test battery.

Item	Specification
Cathode material	$LiNi_{0.5}Co_{0.2}Mn_{0.3}O_2$ (NCM523)
Anode	Graphite
Nominal capacity	2600 mAh
Nominal voltage	3.6 V
Voltage	Charge: 4.2 V Discharge: 2.75 V
Cell mass	44.8 ± 0.2 g
Storage temperature	1 year: −20~25 °C 3 months: −20~45 °C 1 month: −20~60 °C

2.2. Experimental Setup

A schematic diagram of the Altitude Temperature Chamber was utilized to simulate aviation conditions, as shown in Figure 1. The chamber was composed of internal and external cabins. The internal ambient temperature was gradually cooled to the selected temperature by decreasing the external ambient temperature, which was manipulated via the control panel. The chamber interior dimensions were 800 × 600 × 1000 mm, it could maintain internal pressure from low pressure (20 kPa) to atmospheric pressure (101 kPa), and the temperature control window ranged from −20 °C to 70 °C with an accuracy of 1 °C. The experimental chamber was made of stainless-steel panels and was coated with ultrafine glass wool to guarantee temperature precision. In addition, the exterior chamber heated or cooled the interior chamber to maintain a constant ambient temperature, and the ambient pressure was monitored using a pressure sensor in real time. Prior to the tests, the chamber pressure primarily decreased to the selected value and remained stable for a while. Then, the ambient temperature was reduced to the fixed temperature.

To simulate thermally failed cell heat transfer to adjacent cells, a cylindrical heater with 100 W, which had the same dimensions as the 18,650 cell, was employed. The heater was cleaned with residue after each experiment to minimize the influence of ejecta. A K-type thermocouple, with a diameter of 1 mm and an accuracy of 0.5 °C, was attached to the center of the cell to monitor the cell temperature variations synchronously. In addition, the jet flame temperature distribution was measured by a thermocouple tree, which was positioned along the central axis in the vertical direction. The distance interval

was 10 cm. The whole experimental process temperature variations were recorded by the data acquisition equipment NI cDAQ-9213, National Instruments, USA. The mass variations before and after the experiment were determined using an electronic balance (Metter Toledo XP10002S, Metter Toledo, Switzerland) with a resolution of 0.01 g. A SONY FDR-AX700 digital camera (Sony) was employed to capture the thermal runaway behavior and burning process. In addition, the micromorphology and composition of the electrode materials were obtained using the scanning electron microscope (Gemini SEM 450, Zeiss, German) and energy dispersive spectrometer EDS (ESCALAB 250Xi, Thermo Fisher, USA) in this work, respectively.

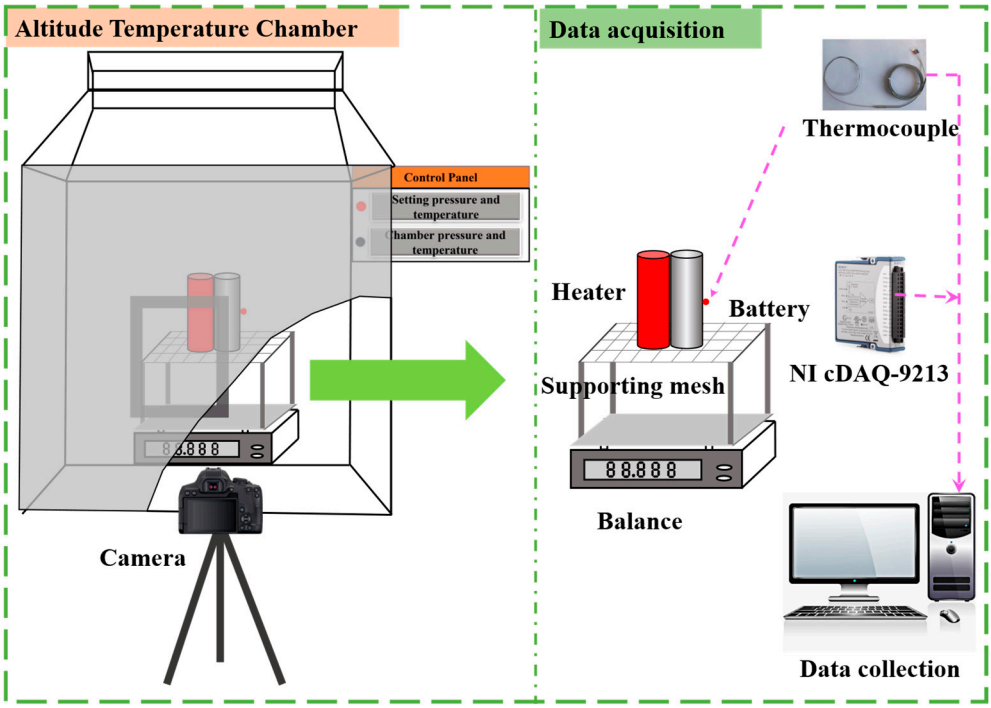

Figure 1. Schematic of the experimental setup.

2.3. Experimental Design and Procedure

Before closing the altitude temperature chamber to start the experiments, the prepared battery was placed on the supporting mesh, and the recording and collection devices were in a state of preparedness. When the internal pressure and temperature reached the setpoint, the cell with 100% SOC was kept in the chamber for 2 h to maintain the lithium-ion battery temperature the same as the chamber's internal conditions [24]. Then, the heater was initiated until a fire or explosion was observed, and all the data acquisition systems were activated simultaneously.

In this work, two key parameters were controlled.

Parameter I. Ambient temperature (T_0).

The performance of lithium-ion batteries is sensitive to the environmental temperature during operation and transportation. In this work, experiments were carried out at various ambient temperatures (−15 °C represents low-temperature conditions and 25 °C represents the optimum temperature) to explore the influence of ambient temperature on thermal behavior at low temperatures.

Parameter II. Ambient pressure (P_0).

The experiments were conducted under three pressure values: 101 kPa represents atmospheric pressure and 40 kPa represents low pressure. The altitude temperature chamber is capable of maintaining stable ambient temperature and pressure simultaneously.

The detailed experimental configurations are illustrated in Table 2. To reduce the effects of thermal runaway gas ejection on the oxygen concentration and pressure, the

chamber door was opened to recover to the previous situation after each test. Finally, all the tests were repeated at least three times to reduce experimental errors.

Table 2. Experimental configurations.

Group No.	Test No.	Temperature (°C)	Pressure (kPa)	SOC (%)	Heating Power (W)
I	1	25	101	100	100
	2		70		
	3		40		
II	4	0	101	100	
	5		70		
	6		40		
III	7	−15	101	100	
	8		70		
	9		40		

3. Results and Discussion

3.1. Thermal Runaway Process of Lithium-Ion Batteries

Figure 2 illustrates the contrasting thermal runaway phenomena of lithium-ion batteries at various ambient pressures and temperatures, where 101 kPa, 25 °C represents the terrestrial environment, which is also the optimum condition for lithium-ion battery operation, and 40 kPa, −15 °C represents the extreme environment of high-altitude aviation conditions. It can be found that the thermal runaway process can be divided into five stages: (I) heating and safety venting, (II) gas release, (III) explosion, (IV) combustion after thermal runaway, and (V) abatement.

In stage I, the cell temperature rose smoothly and was heated by the electric heater on an ongoing basis. As the cell temperature continuously rose, a chain of side reactions accompanied by gas generation occurred inside the cell [25,26]. The internal reaction gases were generated and accumulated continuously. Gradually, the safety valve was unable to withstand the high pressure, which triggered the safety valve to break. A large number of flammable gases, including CO_2, CO, alkane, and electrolyte vapor were released in stage II. However, the temporary cooling was not enough to depress the self-heating process. At this point, the flammable gases and internal electrode active materials started to react with the air, and the influence of the oxygen concentration gradually emerged. Once the cell surface temperature exceeded 200 °C, a chain of side reactions was triggered and released large amounts of heat, resulting in the surface temperature increasing exponentially in stage III. High-temperature sparked or high-speed particles are likely to become the ignition sources of jet fires. However, as the ambient temperature and pressure decreased, the oxygen reduction and heat loss weakened the thermal runaway intensity. It can be seen that the thermal runaway jet fire at 101 kPa, 25 °C was brighter than that at 40 kPa, −15 °C, which demonstrated more intense internal side reactions and exhibited great thermal hazards, as shown in Figure 2 [27]. Subsequently, the residual electrolyte burned steadily for a while at 101 kPa, 25 °C. However, only a weak flame was observed at 40 kPa, −15 °C in stage IV. This phenomenon can be attributed to the following two aspects. On the one hand, as the ambient pressure decreased, the reduced oxygen concentration gradient slowed the air diffusion rate. Therefore, the internal exothermic side reactions and explosion were inhibited [19,28]. On the other hand, as the ambient temperature declined, the convection and radiation heat loss also increased and, thus, more heat accumulation was required before thermal runaway. Finally, the recorded surface temperature decreased quickly and cooled gradually in stage V. Therefore, under aviation conditions, the low ambient pressure and low temperature demonstrate an inhibitory effect on the thermal runaway intensity.

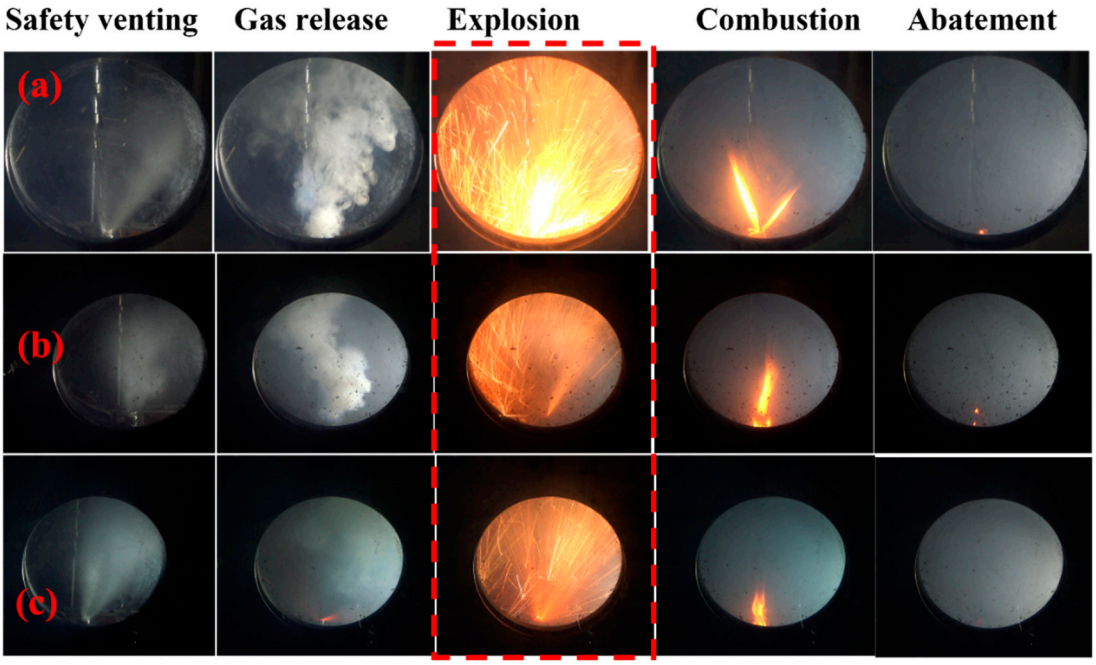

Figure 2. Thermal runaway phenomenon of batteries in aviation conditions: (**a**) 101 kPa, 25 °C, (**b**) 70 kPa, 0 °C, (**c**) 40 kPa, −15 °C.

3.2. Effects of Ambient Pressure

The oxygen concentration and ambient temperature played important roles in the exothermic side reaction and burning process during the thermal runaway process. The oxygen concentration decreased with a decrease in the ambient pressure. The relationship between the oxygen content and ambient pressure can be approximately calculated using the ideal gas law:

$$PV_{chamber} = n_{air}RT \quad (1)$$

Moreover, the oxygen fraction is 21% and remains constant under various pressures. Therefore, the oxygen mole fraction under various pressures in the chamber can be expressed as [21]:

$$n_{O_2} = \frac{0.21 n_{air} PV_{chamber}}{RT_0} \quad (2)$$

where P is the internal chamber pressure, V is the volume of the chamber, n is the air mole number, R is the gas constant, R = 8.314 J/mol/K, and T_0 is the ambient temperature.

To better understand the thermal runaway behaviors, Figure 3a demonstrates the cell temperature profiles under different pressure conditions with the optimum temperature of 25 °C. The other ambient temperatures at various pressures showed a similar trend. In general, lowering the ambient pressure, on the one hand, alleviated the thermal runaway intensity. On the other hand, it postponed the thermal runaway process. It can be noted that the cell surface temperature escalated smoothly, and the average temperature rate was approximately 0.38 °C/s. The ambient pressure had no significant effect on this process. As the safety valve opened, the cell temperature decreased slightly, which could migrate the thermal runaway process to some extent. However, the oxygen gradually penetrated the cell and triggered a chain of exothermic reactions. The impact of the environmental pressure was mainly manifested in the period from the safety valve opening to thermal runaway. Therefore, the ambient oxygen content reduced as the pressure decreased, as illustrated in Equation (2), while the intense thermal runaway entailed airborne oxygen supporting internal exothermic reactions from safety valve rupture to thermal runaway occurrence. Although the ternary cathode materials of lithium-ion batteries can decompose and generate oxygen at approximately 210 °C [29], the mole fraction is too small to influence

the thermal behavior. The decomposition reaction of the NCM 523 cathode material is shown in Equation (3) [30].

$$\mathrm{NCM}(R3-m) \underset{\Delta T,\mathrm{solv}}{\rightarrow} (\mathrm{Mn,\ Ni})\mathrm{O}(Fm3m) + \mathrm{CaO\ (s)} + \mathrm{Ni\ (s)} + \mathrm{O_2\ (g)} \quad (3)$$

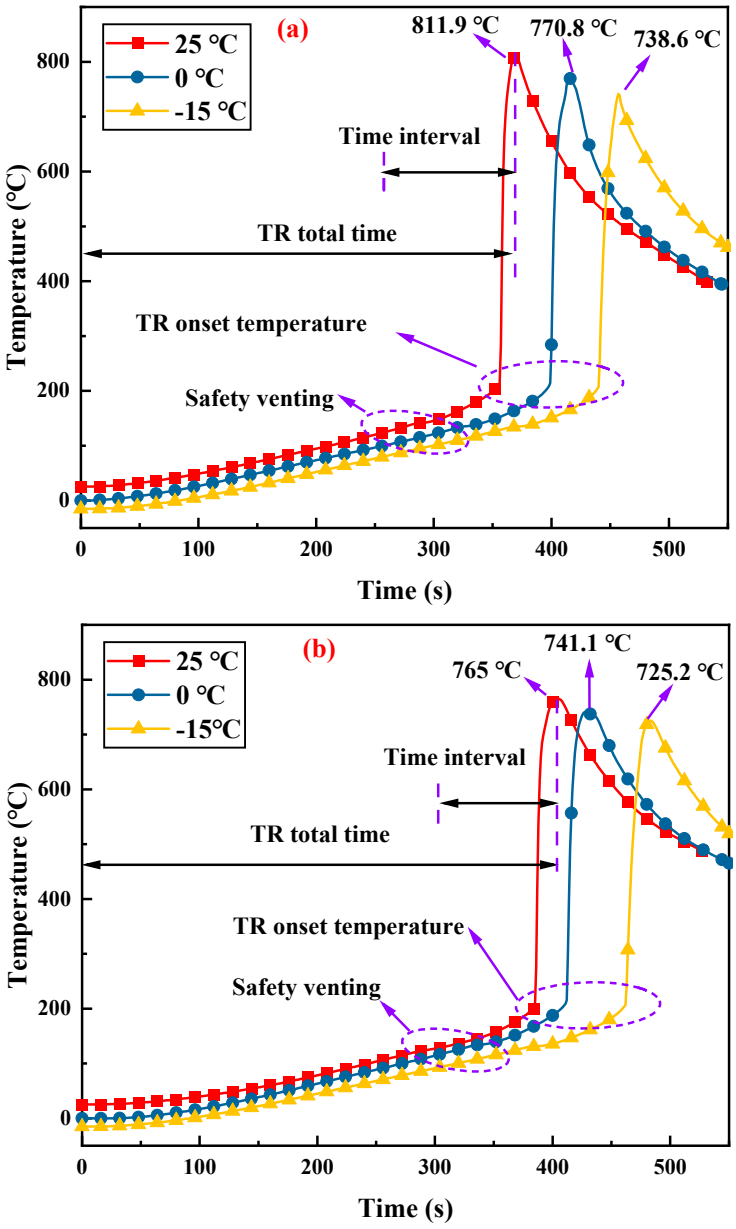

Figure 3. The cell surface temperature variations: (**a**) typical surface temperature at 25 °C under different ambient pressures, (**b**) typical surface temperature at 70 kPa with different ambient temperatures.

Tables 3 and 4 demonstrate the total time (t_{total}) and time interval (Δt) during thermal runaway. The total time is the period from heating to when the lithium-ion battery reaches the maximum temperature, and Δt is the time interval from safety valve rupture to the maximum temperature, which can be expressed using Equation (4) [31]. As the ambient pressure decreased from 101 kPa to 40 kPa, the thermal runaway intensity was alleviated, and the maximum temperature decreased at low ambient pressure, which is consistent with previous works [32]. In addition, the total time to thermal runaway increased from 370 s to 429 s with an increment of 14%. Meanwhile, the time interval, Δt, increased from 71 s to 98 s, an increase of approximately 28%, indicating the predominant effect after the

safety valve opening. Therefore, the increase in the total time and the time interval revealed the inhibitory effect at low pressure.

Table 3. The total thermal runaway time.

Ambient Temperature (°C)	101 kPa (s)	70 kPa (s)	40 kPa (s)
25	370 ± 16.3	415 ± 16.7	460 ± 5.6
0	405 ± 13.9	428 ± 8.1	483 ± 9.5
−15	429 ± 17.6	458 ± 11.9	503 ± 10.8

Table 4. Time interval, Δt, from safety venting to thermal runaway.

Ambient Temperature (°C)	101 kPa (s)	70 kPa (s)	40 kPa (s)
25	75 ± 3.3	89 ± 2.7	98 ± 5.6
0	82 ± 1.9	94 ± 4.1	101 ± 3.5
−15	88 ± 7.6	99 ± 3.9	105 ± 6.8

However, it is different from the primary depression effect on the safety valve opening. The cooling effect of ambient temperature acts on the whole thermal runaway process. At low temperatures, the cell and heating rod remained at a lower initial temperature, which required more time to preheat and trigger thermal runaway. The convection and radiation heat loss increased with decreasing ambient temperature. Figure 3b illustrates the surface temperature evolution at −15 °C, 0 °C, and 25 °C under 70 kPa. It can be seen that the thermal runaway process was postponed at low temperatures, and the total time to thermal runaway increased from 405 s to 483 s, which was an increase of 16%, and the ambient temperature decreased from the optimum temperature of 25 °C to −15 °C. In addition, the time interval ascended from 89 s to 99 s, which was an increase of approximately 10%, demonstrating the predominant inhibiting effect of ambient pressure between venting and the thermal runaway onset time. Finally, it is worth noting that the thermal runaway intensity was weakened at low temperatures; the maximum temperature decreased as the ambient temperature decreased. Therefore, the lower ambient temperature could also decrease the thermal runaway propensity by accelerating the volatilization of the flammable electrolyte.

$$\Delta t = t_{tr} - t_v \tag{4}$$

where t_{tr} is the time to thermal runaway, and t_v is the time for safety venting.

3.3. Thermal Runaway Critical Temperature

To further analyze the thermal runaway characteristics under low-pressure and low-temperature conditions, the critical temperatures including the voltage drop temperature, $T_{v\text{-}drop}$, the safety venting temperature, T_v, the onset temperature, T_{tr}, and the thermal runaway maximum temperature, T_{max} were extensively applied to assess the thermal hazard of the lithium-ion battery [33]. $T_{v\text{-}drop}$ is the temperature at which the voltage drops to 0 V instantly, simultaneously forming an internal short circuit and releasing an amount of joule heat that further accelerates the thermal runaway process. T_v is the corresponding temperature for the safety valve opening from recording videos and the temperature profile decrease. The thermal runaway onset temperature, T_{tr}, is identified as $dT{\cdot}dt^{-1} > 10$ °C/s, which considers the gradient of the cell temperature [34] combined with visual and audible observations, as shown in Equations (5) and (6). T_{max} is the surface maximum temperature that manifests the thermal hazard and intensity during the thermal runaway process, as demonstrated in Equations (7) and (8) [35]. Figure 4 summarizes the critical temperatures of $T_{v\text{-}drop}$, T_v, T_{tr}, and T_{max} under different ambient temperatures and pressures. Supervising voltage fluctuation is one of the most efficient instruments for the early detection of thermal runaway, and internal short circuit formation is closely

associated with the polymer separator property. The temperature for the voltage decrease was approximately 117.4 ± 2 °C, which is insensitive to the ambient temperature and pressure. This result is consistent with previous related works [32]. In addition, as the side reaction proceeded, when the internal pressure of the cell reached the threshold [6,36], the safety valve broke and a portion of gas was released. Previous studies have confirmed that the safety venting temperature is primarily related to the cathode material, SOC, and even the external pressure. However, as shown in Figure 4, the safety venting temperature, T_v, was approximately 135.8 ± 2.7 °C, and the aviation conditions of low temperature and low pressure have no obvious influence.

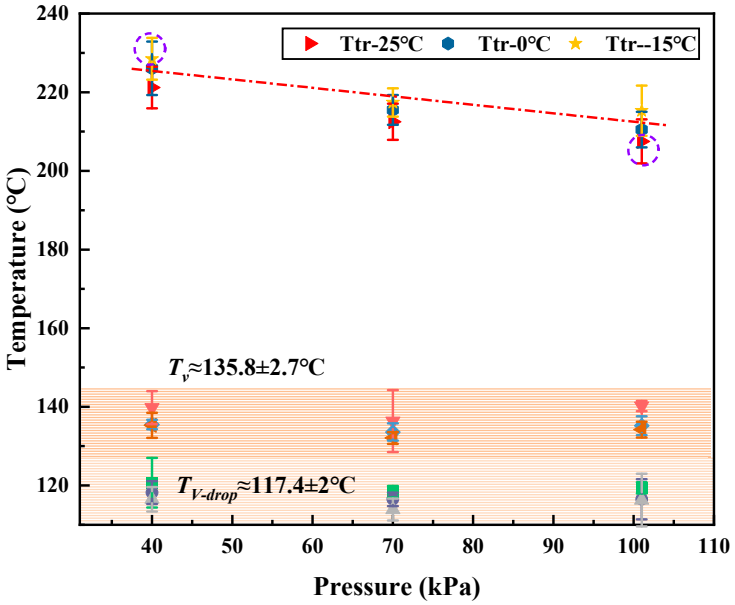

(**a**) The critical temperature of voltage, safety venting, and onset temperature.

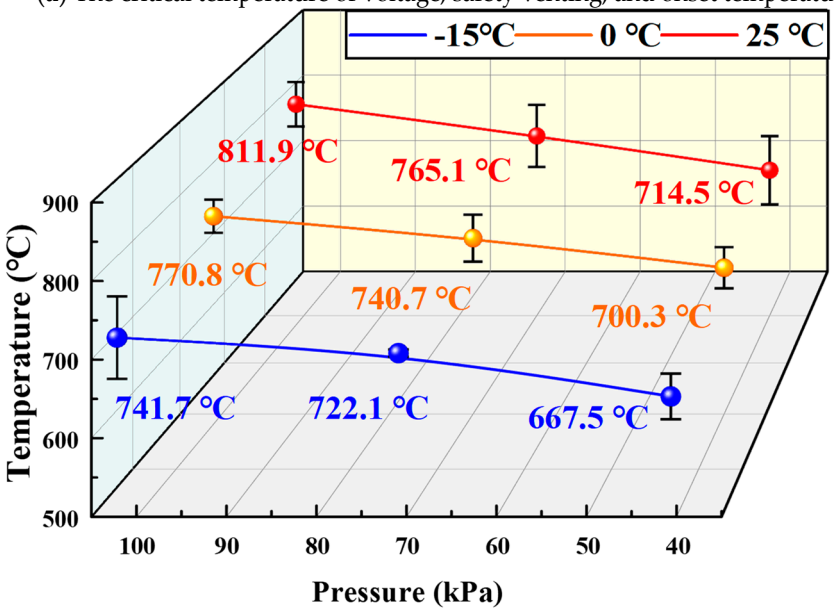

(**b**) The maximum temperature under different conditions.

Figure 4. The critical temperature of voltage drop ($T_{v\text{-}drop}$), safety venting ($T_{venting}$), thermal runaway onset temperature (T_{onset}), and maximum surface temperature (T_{max}) under different conditions.

Thermal runaway onset temperature, T_{tr}, is the turning point at which the cell surface temperature transforms from the gently built-up stage to the dramatic exponential growth stage. It is critical for evaluating battery safety and thermal hazards. In this study, the

thermal runaway onset temperature increased with decreasing ambient pressure and temperature. For example, the thermal runaway onset temperature was 228.2 ± 5.3 °C under 40 kPa, −15 °C, which is higher than 207.5 ± 5.6 °C under the 101 kPa, 25 °C condition. Namely, it is more difficult to trigger thermal runaway under low ambient pressure and temperature. Therefore, it is significant to improve the onset temperature to delay the thermal runaway process. In addition, lowering the pressure reduced the oxygen concentration involved in the internal exothermic reaction, and the low temperature increased the convection and radiation heat loss during thermal runaway. Consequently, a lower maximum temperature was performed for the cell under the coupled effects of low pressure and low temperature. For example, the maximum temperature was 811.9 ± 32.8 °C at 101 kPa, 25 °C, while it was only 667.5 ± 28.8 °C at 40 kPa, −15 °C, which varied by about 144.4 °C. Therefore, low pressure and low temperature have a significant effect on the critical temperature parameters T_{tr} and T_{max}, while the effects on the voltage drop, $T_{v\text{-}drop}$, and safety venting, T_v, are negligible.

$$t_{tr} = \min\{k : T(k+1) - T(k) > 10\ ^\circ\mathrm{C}\} \tag{5}$$

$$T_{tr} = T(t_{tr}) \tag{6}$$

$$t_{\max} = \underset{n}{\operatorname{argmax}}\{T(k)\} \tag{7}$$

$$T_{\max} = \max_{n}\{T(k)\} \tag{8}$$

In addition, the heat transfer process is mainly determined by the cell temperature gradient [37,38]. To further explore the influence of ambient pressure and temperature on the thermal runaway intensity, Figure 5 presents the temperature rate variations at two selected typical pressures and temperatures. It can be seen that the maximum temperature rate even reached 153.1 °C·s^{-1}at 101 kPa, 25 °C, while it was only 57.8 °C·s^{-1}at 40 kPa, −15 °C, a reduction of nearly 2.6 times. The maximum temperature rates with all the experimental conditions are demonstrated in Table 5. A higher maximum temperature rate indicated a more severe thermal runaway. Consequently, combined with the dual effects of ambient pressure and temperature, low pressure with less oxygen content and low temperature with more heat loss can weaken the intensity of exothermic side reactions and lower heat accumulation, which alleviates the thermal runaway intensity.

Table 5. The cell maximum temperature rate of all experimental tests.

Ambient Pressure (kPa)	**25 °C (°C·s^{-1})**	**0 °C (°C·s^{-1})**	**−15 °C (°C·s^{-1})**
101	153.1	107.9	71.6
70	131.5	97.1	68.9
40	98.6	68.8	57.8

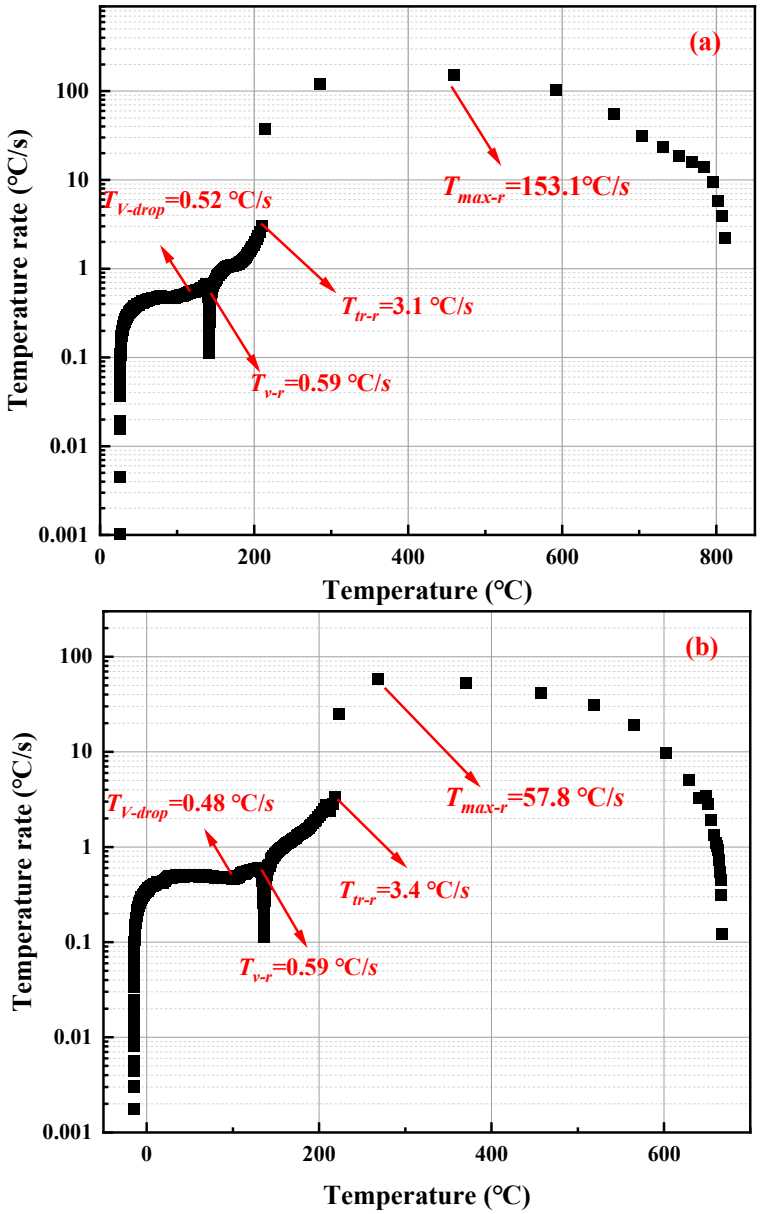

Figure 5. Temperature rate evolution under different conditions: (**a**) temperature rate at 101 kPa, 25 °C; (**b**) temperature rate at 40 kPa, −15 °C.

3.4. Flame Temperature Distribution

To quantify the influence of ambient pressure and temperature on the jet fire. Figure 6 presents the thermal runaway axial temperature distributions of jet fire at 101 kPa, 25 °C and 40 kPa, −15 °C. It can be observed that the flame temperature at 1 cm height presented the maximum values, and the flame temperatures were much higher than the cell surface temperature. For example, the peak flame temperature decreased from 975.7 °C to 696.3 °C, which declined by 28.6% as the ambient pressure and temperature decreased from 101 kPa, 25 °C to 40 kPa, −15 °C. The results demonstrated that both low ambient pressure and temperature can broadly inhibit lithium-ion battery jet fires. For other height flame temperatures in the vertical direction, there was no specific trend at various pressures and temperatures due to the randomness of jet fire. In addition, it should be noted that the farthest location (approximately 20 cm) flame temperature even reached about 187.3 °C, which is sufficient to induce adjacent cell thermal runaway. Therefore, lithium-ion battery thermal runaway may also trigger catastrophic accidents during air transportation.

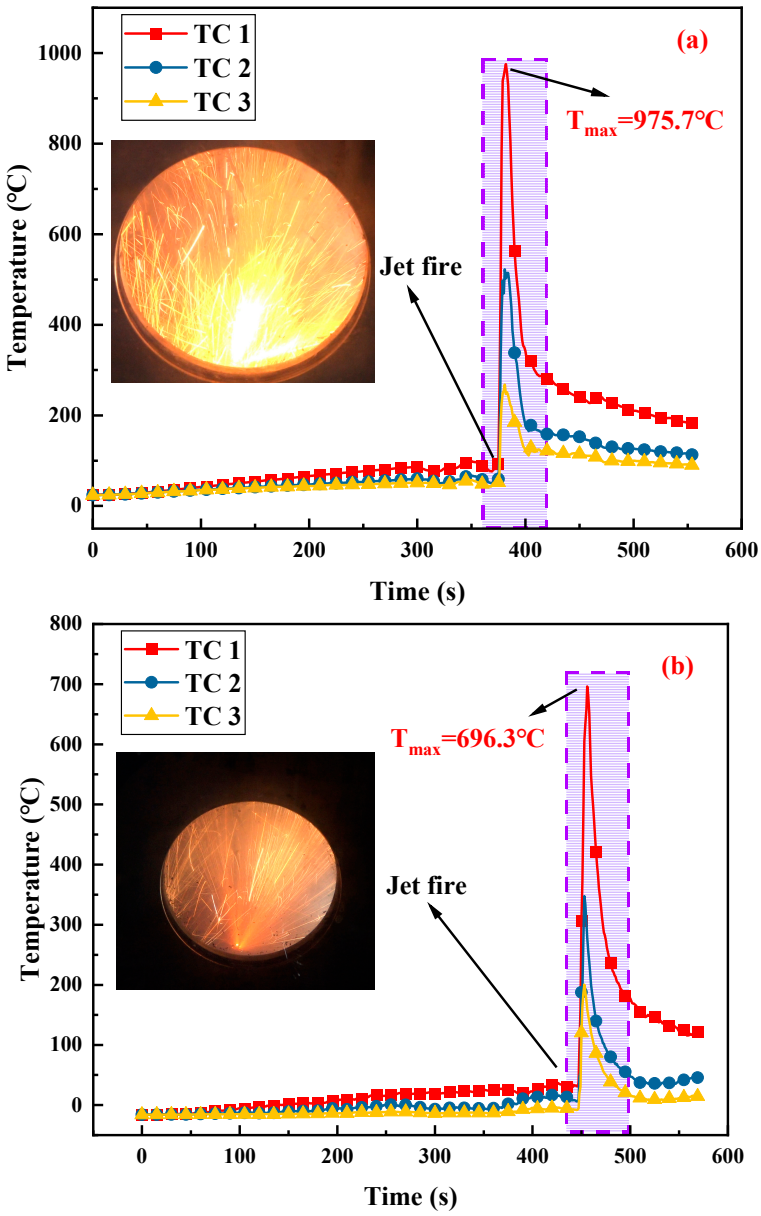

Figure 6. The axial jet fire temperature distributions during thermal runaway. (**a**) 101 kPa, 25 °C, (**b**) 40 kPa, −15 °C.

3.5. Physical and Chemical Characteristics of Debris

A detailed analysis of the changes in the composition of cell active materials before and after thermal runaway can help provide insight into the mechanism of lithium-ion battery thermal runaway. Figure 7 presents a comparison of anode and cathode residues of lithium-ion batteries through the energy dispersive spectrometer (EDS) coupled with field emission scanning electron microscopy (SEM). By disassembling the experimental samples, it was noted that the fresh battery layers were relatively smooth, and the separator acted as an isolation layer to prevent internal short circuits [39]. However, the electrode active materials and electrolytes were consumed, and the cathode and anode were mixed together after thermal runaway. The anode materials of the cell were brittle and easily detached from the Cu current collector. The micromorphology of the electrode materials became rough, and many cracks formed. There was no clear-cut distinction of electrode material morphology between 101 kPa, 25 °C and 40 kPa, −15 °C. In addition, it was found that the deformation of the cathode was more severe than that of the anode and was driven by the high temperature. The aluminum current collector almost melted, and the cathode material

changed from a layered structure to a spine structure and decomposed to release oxygen, and it finally transformed into a rock salt structure [40].

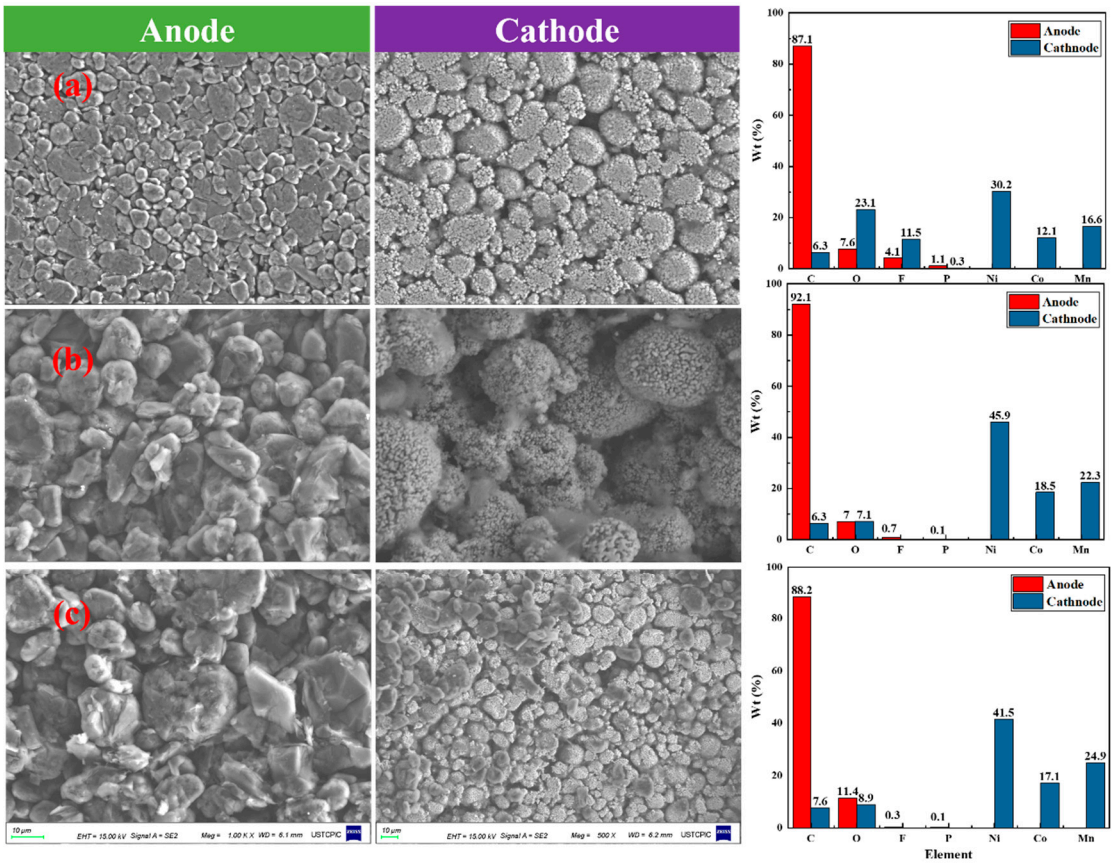

Figure 7. Chemical analysis of the battery before and after thermal runaway. (**a**) fresh battery; (**b**) 101 kPa, 25 °C; (**c**) 40 kPa, −15 °C.

EDS was applied to further analyze the elemental composition of the electrode materials. For the fresh battery, the anode elemental composition mainly included 87% C, 7.6% O, 4.1% F, and 1.1% P. The composition of the cathodes was 30.2% Ni, 12.1% Co, 16.6% Mn, 6.3% C, 23.1% O, 11.5% F, and 0.3% P. After thermal runaway, the anode proportion of the element C increased from 87.1% for the fresh battery to 92.1% at 101 kPa, 25 °C and 88.2% at 40 kPa, −15 °C. A higher degree of carbonization and carbon content at 101 kPa, 25 °C manifested more intense side reactions and combustion behaviors during thermal runaway. Nevertheless, the cathode elements F and P presented similar declining trends and decreased significantly after thermal runaway. For example, the content of F decreased from 11.5% for the fresh battery to nearly 0 at both 101 kPa, 25 °C and 40 kPa, −15 °C, and P reduced from 0.3% to 0.1%. The decrease in the elements F and P indicated that the electrolyte salt, $LiPF_6$, and the binder were consumed in the redox reduction reactions, and a lower F content indicated more intense exothermic reactions inside the cell during thermal runaway.

3.6. Mass Loss

The ejection and burning of the electrolyte and electrode material are the major sources of mass loss during thermal runaway. Lithium-ion batteries with more intense internal reactions exhibited a higher mass loss. Figure 8 illustrates the mass loss at various temperatures and pressures after thermal runaway. It can be noted that the mass loss decreased with decreasing ambient pressure and temperature. For example, as the ambient pressure decreased from 101 kPa to 40 kPa at 0 °C, the mass loss for 100% SOC cells declined from

23.3 g to 19.5 g, which agrees with the experimental results of previous research. The lower oxygen concentration and combustion were primarily responsible for this phenomenon in which more active materials were ejected and combusted during the thermal runaway process. Similarly, as the ambient temperature decreased from 25 °C to −15 °C under 101 kPa, the increasing heat loss and relatively low initial temperature inhibited the intensity of the internal side reactions and burning behaviors, resulting in the mass loss decreasing from 24.1 g to 21.6 g. Therefore, the mass loss outcomes further confirmed that reducing ambient temperature and pressure can weaken the degree of side reaction hazards to some extent, which is chiefly attributed to the variation in the oxygen concentration (ambient pressure) and heat loss (convection and radiation loss) during thermal runaway.

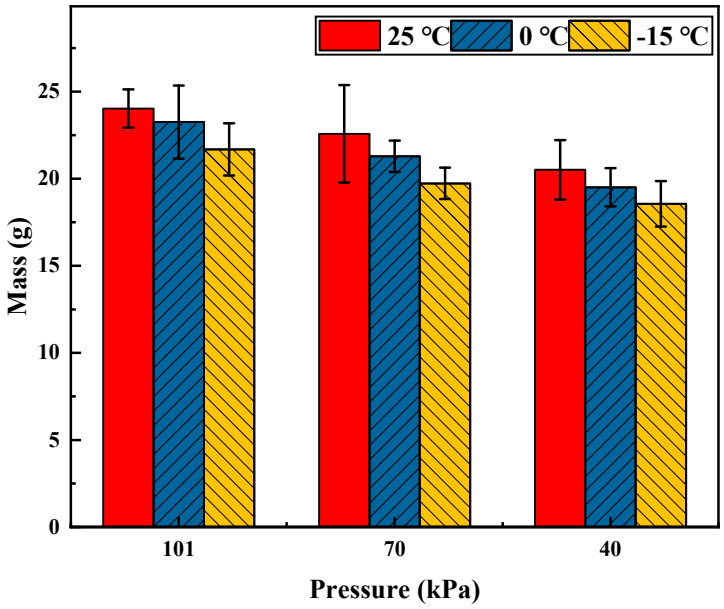

Figure 8. Mass loss of cells after thermal runaway.

4. Conclusions

This work comprehensively probed the thermal characteristics of 18,650 lithium-ion batteries at different ambient pressures and temperatures in an altitude temperature chamber. In this work, the dynamic pressure conditions of 101 kPa, 70 kPa, and 40 kPa and ambient temperatures of −15 °C, 0 °C, and 25 °C were selected. Some critical parameters of lithium-ion batteries, such as temperature variation, mass loss, and heat distribution, were obtained. SEM/EDS tests were utilized to demonstrate the changes in electrode active materials. These results are beneficial to further comprehend the lithium-ion battery thermal characteristics at low-temperature and low-pressure conditions. The primary conclusions are summarized as follows:

The thermal runaway process of a single cell primarily comprises five stages: (I) venting, (II) gas release, (III) explosion, (IV) combustion, and (V) abatement at low temperature and pressure conditions. Remarkably, the venting stage can be regarded as the far-reaching period for thermal runaway. The results indicated that the cell with 100% SOC, a voltage drop temperature of 117.4 ± 2 °C, and a safety venting temperature of 135.8 ± 2.7 °C was insensitive to ambient temperature and pressure. Lowering the pressure can largely attenuate the thermal runaway intensity of lithium-ion batteries, as the oxygen concentration is critical for the successive exothermic reactions and burning process. Meanwhile, as the ambient temperature decreased, the cell with a relatively low initial temperature and more heat loss also postponed and depressed the thermal runaway process. Therefore, as the ambient temperature and pressure decreased, the weak exothermic reactions and slow heat accumulation resulted in a higher thermal runaway onset temperature, a lower maximum temperature and temperature rate, and a lower mass loss. Such a phenomenon was further

verified through SEM/EDS analysis of the electrode materials, where the elements F and P decreased significantly after thermal runaway. In this work, the mechanism of pressure and temperature on thermal runaway was investigated, which could deepen our understanding of thermal runaway characteristics under extreme conditions and help to improve the fire safety of cells during air transportation.

Author Contributions: D.M.: Conceptualization, Writing—original draft, Formal analysis, Investigation. J.W. (Jingwen Weng): Methodology, Writing—review &editing. J.W. (Jian Wang): Conceptualization, Methodology, Writing—review. All authors have read and agreed to the published version of the manuscript.

Funding: The authors acknowledge the support of the Guangdong Basic and Applied Basic Research Foundation (2021B1515130008) and The Science and Technology Program of the Fire and Rescue Department Ministry of Emergency Management of China (2022XFZD12).

Data Availability Statement: The original contributions presented in the study are included in the article, further inquiries can be directed to the corresponding author.

Conflicts of Interest: The authors declare that they have no known competing financial interests or personal relationships that could have appeared to influence the work reported in this paper.

References

1. Epstein, A.; O'Flarity, S. Considerations for Reducing Aviation's CO_2 with Aircraft Electric Propulsion. *J. Propuls. Power* **2019**, *35*, 1–11. [CrossRef]
2. Niu, H.; Chen, C.; Liu, Y.; Li, L.; Li, Z.; Ji, D.; Huang, X. Mitigating thermal runaway propagation of NCM 811 prismatic batteries via hollow glass microspheres plates. *Process Saf. Environ. Prot.* **2022**, *162*, 672–683. [CrossRef]
3. Liu, P.; Sun, H.; Qiao, Y.; Sun, S.; Wang, C.; Jin, K.; Mao, B.; Wang, Q. Experimental study on the thermal runaway and fire behavior of $LiNi_{0.8}Co_{0.1}Mn_{0.1}O_2$ battery in open and confined spaces. *Process Saf. Environ. Prot.* **2022**, *158*, 711–726. [CrossRef]
4. Xie, S.; Yang, X.; Sun, Q.; Wang, Z.; He, Y. Research progress and prospects on thermal safety of lithium-ion batteries in aviation low-temperature and low-pressure environments. *J. Energy Storage* **2024**, *83*, 110734. [CrossRef]
5. Shao, Q.; Yang, M.; Xu, C.; Wang, H.; Liu, H. Fire Risk Analysis of Runway Excursion Accidents in High-Plateau Airport. *IEEE Access* **2020**, *8*, 204400–204416. [CrossRef]
6. Mao, B.; Zhao, C.; Chen, H.; Wang, Q.; Sun, J. Experimental and modeling analysis of jet flow and fire dynamics of 18650-type lithium-ion battery. *Appl. Energy* **2021**, *281*, 116054. [CrossRef]
7. Li, J.-H.; Wu, J.; Yu, Y.-X. Toward Large-Capacity and High-Stability Lithium Storages via Constructing Quinone–2D-MnO_2-Pillared Structures. *J. Phys. Chem. C* **2021**, *125*, 3725–3732. [CrossRef]
8. Pigłowska, M.; Kurc, B.; Rymaniak, Ł. Starch as the Flame Retardant for Electrolytes in Lithium-Ion Cells. *Materials* **2022**, *15*, 523. [CrossRef]
9. Xie, S.; Ren, L.; Gong, Y.; Li, M.; Chen, X. Effect of Charging/Discharging Rate on the Thermal Runaway Characteristics of Lithium-Ion Batteries in Low Pressure. *J. Electrochem. Soc.* **2020**, *167*, 140503. [CrossRef]
10. Zhu, N.; Wang, X.; Chen, M.; Huang, Q.; Ding, C.; Wang, J. Study on the combustion behaviors and thermal stability of aging lithium-ion batteries with different states of charge at low pressure. *Process Saf. Environ. Prot.* **2023**, *174*, 391–402. [CrossRef]
11. Meng, H.; Yang, Q.; Zio, E.; Xing, J. An integrated methodology for dynamic risk prediction of thermal runaway in lithium-ion batteries. *Process Saf. Environ. Prot.* **2023**, *171*, 385–395. [CrossRef]
12. Wang, X.; Liu, Y.; Song, C.; Gao, L. Characteristics of oxygenic-thermal coupled jet driven by concentration difference and temperature difference at high altitudes. *Build. Environ.* **2023**, *228*, 109897. [CrossRef]
13. Bills, A.; Sripad, S.; Fredericks, W.L.; Singh, M.; Viswanathan, V. Performance Metrics Required of Next-Generation Batteries to Electrify Commercial Aircraft. *ACS Energy Lett.* **2020**, *5*, 663–668. [CrossRef]
14. Warren, M.; Garbo, A.; Kotwicz Herniczek, M.T.; Hamilton, T.; German, B. Effects of Range Requirements and Battery Technology on Electric VTOL Sizing and Operational Performance. In Proceedings of the AIAA Scitech 2019 Forum: American Institute of Aeronautics and Astronautics, San Diego, CA, USA, 7–11 January 2019.
15. Chen, M.; Zhou, D.; Chen, X.; Zhang, W.; Liu, J.; Yuen, R.; Wang, J. Investigation on the thermal hazards of 18650 lithium ion batteries by fire calorimeter. *J. Therm. Anal. Calorim.* **2015**, *122*, 755–763. [CrossRef]
16. Chen, M.; Ouyang, D.; Weng, J.; Liu, J.; Wang, J. Environmental pressure effects on thermal runaway and fire behaviors of lithium-ion battery with different cathodes and state of charge. *Process Saf. Environ. Prot.* **2019**, *130*, 250–256. [CrossRef]
17. Weng, J.; Yang, X.; Ouyang, D.; Chen, M.; Zhang, G.; Wang, J. Comparative study on the transversal/lengthwise thermal failure propagation and heating position effect of lithium-ion batteries. *Appl. Energy* **2019**, *255*, 113761. [CrossRef]
18. Chen, M.; Liu, J.; He, Y.; Yuen, R.; Wang, J. Study of the fire hazards of lithium-ion batteries at different pressures. *Appl. Therm. Eng.* **2017**, *125*, 1061–1074. [CrossRef]

19. Fu, Y.; Lu, S.; Shi, L.; Cheng, X.; Zhang, H. Ignition and combustion characteristics of lithium ion batteries under low atmospheric pressure. *Energy* **2018**, *161*, 38–45. [CrossRef]
20. Liu, Y.; Niu, H.; Xu, C.; Huang, X. Thermal runaway propagation in linear battery module under low atmospheric pressure. *Appl. Therm. Eng.* **2022**, *216*, 119086. [CrossRef]
21. Jia, Z.; Huang, Z.; Zhai, H.; Qin, P.; Zhang, Y.; Li, Y.; Wang, Q. Experimental investigation on thermal runaway propagation of 18,650 lithium-ion battery modules with two cathode materials at low pressure. *Energy* **2022**, *251*, 123925. [CrossRef]
22. Niu, H.; Chen, C.; Ji, D.; Li, L.; Li, Z.; Liu, Y.; Huang, X. Thermal-Runaway Propagation over a Linear Cylindrical Battery Module. *Fire Technol.* **2020**, *56*, 2491–2507. [CrossRef]
23. Guo, L.S.; Wang, Z.R.; Wang, J.H.; Luo, Q.K.; Liu, J.J. Effects of the environmental temperature and heat dissipation condition on the thermal runaway of lithium ion batteries during the charge-discharge process. *J. Loss Prev. Process Ind.* **2017**, *49*, 953–960. [CrossRef]
24. Ouyang, D.; Hu, J.; Chen, M.; Weng, J.; Huang, Q.; Liu, J.; Wang, J. Effects of abusive temperature environment and cycle rate on the homogeneity of lithium-ion battery. *Thermochim. Acta* **2019**, *676*, 241–248. [CrossRef]
25. Wang, Q.; Ping, P.; Zhao, X.; Chu, G.; Sun, J.; Chen, C. Thermal runaway caused fire and explosion of lithium ion battery. *J. Power Sources* **2012**, *208*, 210–224. [CrossRef]
26. Wen, C.-Y.; Jhu, C.-Y.; Wang, Y.-W.; Chiang, C.-C.; Shu, C.-M. Thermal runaway features of 18650 lithium-ion batteries for $LiFePO_4$ cathode material by DSC and VSP2. *J. Therm. Anal. Calorim.* **2012**, *109*, 1297–1302. [CrossRef]
27. Wang, Z.; He, T.; Bian, H.; Jiang, F.; Yang, Y. Characteristics of and factors influencing thermal runaway propagation in lithium-ion battery packs. *J. Energy Storage* **2021**, *41*, 102956. [CrossRef]
28. Weng, J.; Ouyang, D.; Liu, Y.; Chen, M.; Li, Y.; Huang, X.; Wang, J. Alleviation on battery thermal runaway propagation: Effects of oxygen level and dilution gas. *J. Power Sources* **2021**, *509*, 230340. [CrossRef]
29. Huang, Z.; Li, X.; Wang, Q.; Duan, Q.; Li, Y.; Li, L.; Wang, Q. Experimental investigation on thermal runaway propagation of large format lithium ion battery modules with two cathodes. *Int. J. Heat Mass Transf.* **2021**, *172*, 121077. [CrossRef]
30. Mao, B.; Chen, H.; Jiang, L.; Zhao, C.; Sun, J.; Wang, Q. Refined study on lithium ion battery combustion in open space and a combustion chamber. *Process Saf. Environ. Prot.* **2020**, *139*, 133–146. [CrossRef]
31. Ouyang, D.; Weng, J.; Chen, M.; Wang, J. What a role does the safety vent play in the safety of 18650-size lithium-ion batteries? *Process Saf. Environ. Prot.* **2022**, *159*, 433–441. [CrossRef]
32. Liu, Y.; Niu, H.; Li, Z.; Liu, J.; Xu, C.; Huang, X. Thermal runaway characteristics and failure criticality of massive ternary Li-ion battery piles in low-pressure storage and transport. *Process Saf. Environ. Prot.* **2021**, *155*, 486–497. [CrossRef]
33. Meng, D.; Wang, X.; Chen, M.; Wang, J. Effects of environmental temperature on the thermal runaway of lithium-ion batteries during charging process. *J. Loss Prev. Process Ind.* **2023**, *83*, 105084. [CrossRef]
34. Feng, X.; Zheng, S.; Ren, D.; He, X.; Wang, L.; Cui, H.; Liu, X.; Jin, C.; Zhang, F.; Xu, C.; et al. Investigating the thermal runaway mechanisms of lithium-ion batteries based on thermal analysis database. *Appl. Energy* **2019**, *246*, 53–64. [CrossRef]
35. Liu, Q.; Yi, X.; Han, X. Effect of Different Arrangement on Thermal Runaway Characteristics of 18650 Lithium Ion Batteries Under the Typical Pressure in Civil Aviation Transportation. *Fire Technol.* **2020**, *56*, 2509–2523.
36. Yan, H.; Marr, K.C.; Ezekoye, O.A. Towards Fire Forensic Characteristics of Failed Cylindrical Format Lithium–Ion Cells and Batteries. *Fire Technol.* **2021**, *57*, 1723–1752. [CrossRef]
37. Hu, J.; Liu, T.; Tang, Q.; Wang, X. Experimental investigation on thermal runaway propagation in the lithium ion battery modules under charging condition. *Appl. Therm. Eng.* **2022**, *211*, 118522. [CrossRef]
38. Liu, T.; Hu, J.; Tao, C.; Zhu, X.; Wang, X. Effect of parallel connection on 18650-type lithium ion battery thermal runaway propagation and active cooling prevention with water mist. *Appl. Therm. Eng.* **2021**, *184*, 116291. [CrossRef]
39. Ouyang, D.; Weng, J.; Chen, M.; Wang, J. Impact of Charging and Charging Rate on Thermal Runaway Behaviors of Lithium-Ion Cells. *J. Electrochem. Soc.* **2021**, *168*, 120510. [CrossRef]
40. Jung, R.; Metzger, M.; Maglia, F.; Stinner, C.; Gasteiger, H.A. Oxygen Release and Its Effect on the Cycling Stability of $LiNi_xMn_yCo_zO_2$(NMC) Cathode Materials for Li-Ion Batteries. *J. Electrochem. Soc.* **2017**, *164*, A1361–A1377. [CrossRef]